Journal of
Experimental and Theoretical Analyses

MDPI

Article

An Evaluation Method to Estimate a Vehicle's Center of Gravity During Motion Based on Acceleration Relationships

Francisco Castro [1,2,*], Francisco Queirós de Melo [1], David Faria [1], Job Silva [1], João Nunes [1], Pedro José Sousa [1,2], Mário Augusto Pires Vaz [1,2] and Pedro M. G. P. Moreira [1]

[1] INEGI—Institute of Science and Innovation in Mechanical and Industrial Engineering, 4200-465 Porto, Portugal
[2] FEUP—Faculty of Engineering, University of Porto, 4200-465 Porto, Portugal
* Correspondence: fcastro@inegi.up.pt

Abstract

This paper presents a practical and cost-effective method for in-motion estimation of a vehicle's CoG position in all three directions by measuring accelerations during two types of maneuvers: braking (longitudinal and vertical CoG estimation) and cornering (lateral and vertical CoG estimation). The proposed method's main advantage is that it does not require knowledge of vehicle characteristics, such as mass distribution, suspension geometry, or inertia parameters. It relies solely on the known distances between the sensors and their positions relative to a defined reference point on the vehicle. To validate the developed method, experimental tests were conducted on a prototype vehicle, varying the load conditions for the proposed driving scenarios. The CoG position obtained from dynamic maneuvers was compared with reference values derived from static measurements. The results showed that the proposed method could estimate the CoG position with an average error of 3% in the longitudinal direction, a maximum error of 12% in the lateral direction, and a maximum error of 14% in the vertical direction.

Keywords: rollover accidents; vehicle's CoG estimation; vehicle dynamics; vehicle active safety

1. Introduction

The position of a vehicle's center of gravity (CoG) is an important parameter in vehicle dynamics that influences stability, handling, rollover risk, and braking performance [1–6]. Thus, an accurate knowledge of the CoG position can not only improve active safety systems but can also enhance the accuracy of vehicular accident reconstruction, since it allows for a better understanding of dynamic load transfers and vehicle response [7].

Despite its relevance, the CoG position is not often provided by manufacturers, and when it is provided, they provide only the nominal values for inertial properties and CoG position for unloaded conditions. However, this does not reflect real-world operational variations, since it can vary considerably with passenger and cargo loading.

The CoG position is not directly measurable in real-time, and existing approaches rely on complex models or require detailed knowledge of vehicle parameters, limiting their applicability in real-world scenarios. Nevertheless, the estimation of the vehicle's CoG height is a research topic in the context of rollover prevention and vehicle dynamics control. The estimation techniques rely on model-based methods: vehicle roll models [8–17] and vehicle longitudinal models [11,18–20]. On the other hand, different estimation techniques have also been investigated to determine the CoG location more accurately. The most common filtering techniques are the Kalman Filters, including the standard Kalman Filter

Check for updates

Academic Editors: Jingzheng Ren and Marco Rossi

Received: 26 September 2025
Revised: 20 November 2025
Accepted: 5 January 2026
Published: 15 January 2026

Copyright: © 2026 by the authors. Licensee MDPI, Basel, Switzerland. This article is an open access article distributed under the terms and conditions of the Creative Commons Attribution (CC BY) license.

(KF) [15], Extended Kalman Filters (EKFs) [8,16], the Dual Extended Kalman Filter [13], and hybrid approaches which combine the EKF with other variations, such as the Adaptive Kalman Filter (AKF) [20] and the Huber Extended Kalman Filter [19]. Another estimation algorithm that is commonly used for CoG position estimation is Recursive Least Squares (RLS), including its variants, such as Linear Recursive Least Squares (LRLS), as in [11,17], and Fast Fixed Recursive Least Squares (FFRLS), applied in [12]. Moreover, Least Mean Squares (LMS) has also been applied to the estimation process, as in [9], where the authors used Normalized Least Mean Squares (NLMS).

Despite all these achievements, there is still no cost-effective method or standard equipment to evaluate CoG position when a vehicle is in motion that ensures accuracy, low computational burden, and real-time feasibility for a wide range of vehicles and maneuvers. Additionally, all the methods rely on onboard sensors, high-quality sensors, or previously known parameter measurements.

The objective of this study was to develop a methodology to estimate a vehicle's CoG when it is in motion. In order to estimate the CoG position in a x-z plane, a vehicle longitudinal model was developed for a braking maneuver, and to estimate the CoG position in a y-z plane, a vehicle roll model was developed for a cornering maneuver. Thus, for the measurements with the vehicle in motion, it is necessary to determine the accelerations and the angles to which the vehicle body is subjected. Similar approaches were already applied in ships [21], aerial vehicles [22], aircraft [23], and spacecraft [24].

This work extends the multi-accelerometer "center of accelerations" approach to a road vehicle and is based on theoretical aspects of general plane-motion kinematics. The method does not require vehicle parameters (mass distribution, suspension geometry, or inertia parameters) and relies only on the known distances between the sensors and their positions relative to a vehicle reference point. Using two low-cost sensors for the in-motion tests, the method is validated against a static reference for different load cases.

The content of this paper is organized as follows. In Section 2, the methodology developed to estimate the CoG position in motion is presented, as well as the laboratory static setup used to validate the results. Section 3 depicts the experimental test results from the static procedure and from the in-motion road tests for the two approaches, followed by the discussion of all results. In Section 4, the main conclusions are presented, and future work is proposed.

2. Materials and Methods

In a rigid body, the distance between any two points is constant; this property is very important to simplify the kinematic equations of rigid bodies. Let us consider two generic points I and J in a solid S, as shown in Figure 1.

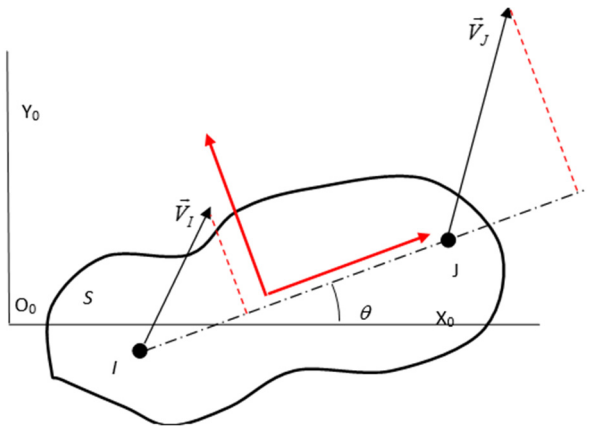


Figure 1. Rigid body in plane motion: projective property of the velocity field.

The vectors $\vec{V_I}$ and $\vec{V_J}$, applied to the points of the solid, respectively, I and J, can refer to displacements, velocities, or accelerations, and their orientation and magnitude are irrelevant. However, their projection onto the line joining the two points of the solid must necessarily be equal (as shown in Figure 1), given that the solid is undeformable. This property of rigid solids in motion is called the projective property of the kinematic field (displacements, velocities, and accelerations). This property makes 2D-kinematic problems of the rigid solid graphically solvable. In any case, using a local reference frame (in which one of the axes can coincide with the line joining two points of the solid), it is possible to establish the kinematic compatibility equations for the displacements, velocities, and accelerations at any point of the solid from just two points. This characteristic is very useful in solving problems involving the shape variation in articulated systems, a subject that will be discussed in detail below. A simple analysis allows us to deduce that a solid in plane motion has two types of displacement: translation (all material points move equally and along the same trajectory) and rotation around an axis.

The kinematics of a rigid solid in plane motion is described by Mozzi's equation, which can be deduced from the figure above:

$$\vec{V_J} = \vec{V_I} + \vec{\omega} \times \vec{IJ} \tag{1}$$

where $\vec{V_I}$ and $\vec{V_J}$ are the absolute velocities in the plane at two points **I** and **J** of the solid, and $\vec{\omega}$ is the angular velocity.

In a plane motion, the acceleration field is obtained by differentiating the previous equation with respect to time.

$$\frac{d\vec{V_J}}{dt} = \frac{d\vec{V_I}}{dt} + \frac{d\vec{\omega}}{dt} \times \vec{IJ} + \vec{\omega} \times \frac{d(\vec{IJ})}{dt} \tag{2}$$

Considering that $\frac{d(\vec{IJ})}{dt}$ is the velocity of point J in relation to I (as if it were rotating around I), which gives

$$\frac{d(\vec{IJ})}{dt} = \omega \times (\vec{IJ}) \tag{3}$$

Thus, upon completing Equation (2), the following equation can be obtained:

$$\frac{d\vec{V_J}}{dt} = \frac{d\vec{V_I}}{dt} + \underbrace{\frac{d\vec{\omega}}{dt}}_{acel.angular} \times \vec{IJ} + \vec{\omega} \times (\omega \times \vec{IJ});$$

$$\vec{A_J} = \vec{A_I} + \vec{\alpha} \times \vec{IJ} + \underbrace{\vec{\omega} \times (\omega \times \vec{IJ})}_{acel.centriptal} \tag{4}$$

In a transient phenomenon, such as braking or accelerating a vehicle (during a brief period of time dt), the angular acceleration generates a small angular velocity (due to the brief integration time) so that the centripetal acceleration portion can be neglected. The angular acceleration contributes to the generation of the centrifugal force component, which generates no inertial moment, as its vector passes through the center of acceleration and is in balance with the body points.

$$\vec{A_J} = \vec{A_I} + \vec{\alpha} \times \vec{IJ} \tag{5}$$

When a vehicle is subjected to an acceleration field and two points are selected for acceleration measurement, the dynamic properties of rigid bodies in motion are essential to obtain the center of accelerations, a point approximately coincident with the center of mass.

To generalize this study, a rigid body with an undetermined shape and volume contour is considered, where it is subjected to an acceleration field, but for a particular analysis, it is assumed that the acceleration field exists in a plane (Figure 2). An important and restrictive condition validating the acceleration field is that the projection property of any vector for displacement, velocity, and acceleration at two points of the solid means that the projection of such vector entities, projected on the line joining the mentioned two points, should be necessarily equal on the connection line at the points.

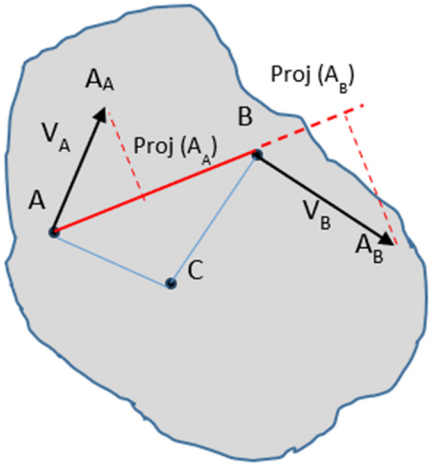


Figure 2. Rigid body motion in generalized kinematics.

The projections of the accelerations at points A and B should be necessarily equal along line AB, otherwise the solid would not be rigid. This is an important assumption for the experimenter to check the condition and eventually question the bonding effectiveness of accelerometers if they are firmly attached to the body surface.

Once this condition is observed, the next step is to obtain the center of acceleration on the plane where two points (A, B) are used to characterize the solid acceleration field. That point has an important property associated, being the center of the vector field, that is, the orthogonality of the acceleration vectors to the respective position vector, as CA and CB in the previous Figure 2. The position of point C is unknown, and its determination is the main goal of the procedure discussed herein.

To characterize the orthogonality of the acceleration vectors AA and AB relative to their position vectors CA and CB, the appropriate calculation is the inner product of each acceleration and position vector:

$$\begin{cases} V_A \cdot CA = 0 \\ V_B \cdot CB = 0 \end{cases} \tag{6}$$

V_A and V_B are vectors where their components in a reference basis are known. On the other hand, the position of point C is not known, so there are two coordinates that are the problem's unknowns. Thus, the solution is achieved by

$$\begin{cases} v_{Ax} \times (A_x - C_x) + v_{Ay} \times (A_y - C_y) = 0 \\ v_{Bx} \times (B_x - C_x) + v_{By} \times (B_y - C_y) = 0 \end{cases} \tag{7}$$

or

$$\begin{cases} v_{Ax} \times (-C_x) + v_{Ay} \times (-C_y) = -v_{Ax} \times A_x - v_{Ay} \times A_y \\ v_{Bx} \times (-C_x) + v_{By} \times (-C_y) = -v_{Bx} \times B_x - v_{By} \times B_y \end{cases} \tag{8}$$

An important remark goes to the instantaneous acceleration at the center of mass: here, the acceleration is only translational in the horizontal direction (without any vertical component), and equal to the projections on the line joining both points A and B, respectively, vectors *Proj* (A_A) and *Proj* (A_B), which are equal. This statement can be extended to any point on the rigid body, since there is no relative change in the distance between points.

The following data are merely didactic and do not correspond to any experimental example. Considering the distance between points A and B to be 1 m, and as a simplification of the problem data, it is assumed that the origin of the Cartesian basis is point A ($A_x = 0$; $A_y = 0$). Also, if the x-axis is assumed to be along the line AB, then B (1, 0). The components of the acceleration vectors are A (10, 10) m/s^2 and B (10, −20) m/s^2.

The projection property of the acceleration vectors should be verified. The solution system is obtained by applying Equation (8):

$$\begin{cases} 10 \times (-C_x) + 10 \times (-C_y) = 0 - 10 \times 0 = 0 \\ 10 \times (-C_x) - 20 \times (-C_y) = -10 \times 1 - 0 \end{cases} \leftrightarrow \begin{cases} -10C_x - 10C_y = 0 \\ -10 \times C_x + 20C_y = -10 \end{cases}$$

Thus, the solution is $C_x = 0.333$ m; $C_y = -0.333$ m.

The translation component of acceleration, particularly at the center of mass, is 10 m/s^2, as expected given the body is rigid.

2.1. Evaluation of the Vehicle's Center of Mass by Experimental Technique

An experimental procedure to estimate the vehicle's center of mass is proposed and implemented. The methodology consists of classical concepts of kinematics and dynamics of rigid solids. It provides a straightforward method, using sensors whose positions are known, to collect data from dynamic parameters of the vehicle model. The method does not demand sharp maneuvers, thus leading to safe operations. An initial description of the theoretical fundamentals is presented, using the vehicle's body model presented in Figure 3.

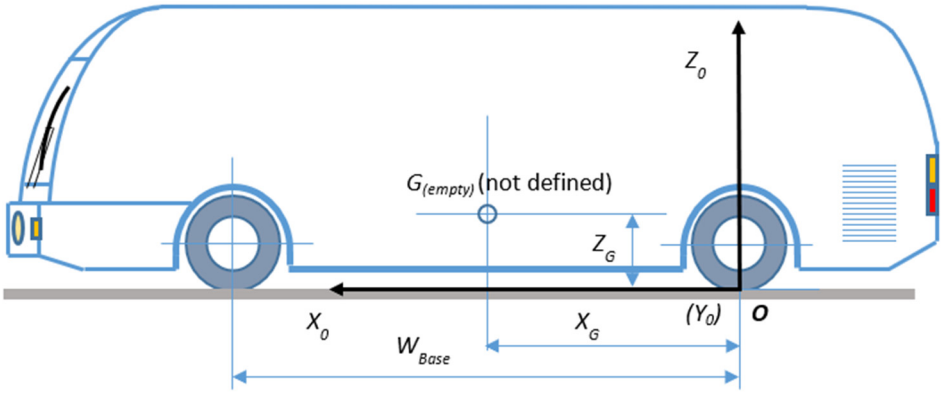


Figure 3. Example of coordinates and points on a generic vehicle dynamic analysis.

As a starting point for addressing the problem, it is necessary to consider Newton's Fundamental Laws of Dynamics, which are the theoretical basis for the solution's development.

1. The resulting vector of a force system acting on a rigid body equals the product of the mass by the acceleration at the body's center of mass.
2. The resulting moment of force vectors and moments is equal to the body's moment of inertia, related to any point of the body, multiplied by the angular acceleration of the body.

In the foregoing analysis, Newton's second law can be implemented considering that the center of mass is coincident with the center of acceleration, as the solid rotations are quite small in this case (corresponding to the vehicle's pitch angle, which is generally small). The vehicle's center of mass moves along a horizontal straight trajectory, thus ensuring that vertical forces are in equilibrium and no vertical acceleration exists.

2.1.1. CoG Estimation (x-z plane) by Longitudinal Accelerations

As previously mentioned, it does not matter whether there is additional load on the vehicle; the position of the center of mass is unique at any moment. The vehicle runs on a straight trajectory at a prescribed speed, followed by braking, which generates a transient acceleration system. The data relevant to the problem's solution are obtained from the accelerometers installed on the vehicle's body.

The following initial assumptions are stated:

1. The vertical forces are solely due to the vehicle's weight, and the resulting force from vertical actions is zero. This is equivalent to stating that the vehicle's weight is balanced by the upward vertical reactions at the wheels in contact with the pavement.
2. The pitch angle of the vehicle due to transient braking forces is small, thus ensuring that the acceleration's center of rotation is effectively coincident with the vehicle's center of mass.

For the experimental evaluation of the CoG position (plane x-z), two 3D accelerometers are installed on top of the vehicle's model, and a braking maneuver is performed (see Figure 4). The recorded data consist of non-zero values along the longitudinal (X_0) and vertical axes (Z_0)—a_{1x}, a_{2x} a_{1z}, a_{2z}, while the lateral (Y_0) acceleration components are expected to be zero (negligible) due to the straight-line motion.

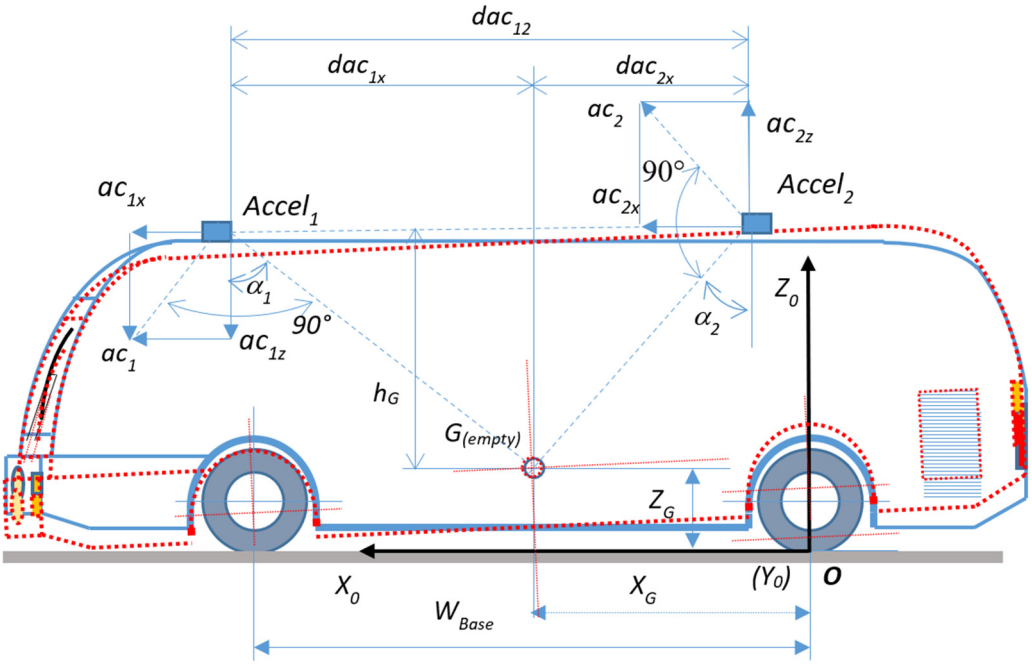


Figure 4. Sketch of a vehicle geometry in a braking motion.

The vehicle's CoG position can be determined using a graphical method by measuring the accelerations, which relies on plotting each resultant acceleration vector and drawing lines perpendicular to those vectors. The intersection point of these two normal lines corresponds to the CoG position on the *x*-*z* plane. This method relies on simple characteristics of a rigid body, which means that under a straight-line motion, the projection of

the acceleration vectors onto the straight line connecting any two points must be equal. If this condition is not met, the body would deform. Then, for a vehicle under a braking maneuver, the condition $|ac_{1x}| = |ac_{2x}|$ must hold. Moreover, as the vehicle is running on a straight trajectory, this property is applied to any point of the vehicle's body for horizontal acceleration vector components.

The analytical formulation of the solution is based on fundamental geometric relations, such as triangle properties. The following assumptions for the method are presented,

- The accelerometer distance dac_{12} is prescribed and known (at points Accel_1 and Accel_2). Since the body is rigid, this distance cannot change. Hence, acceleration vectors projected in the horizontal direction X_0 are necessarily equal.
- By experimental measurements, the angles between acceleration components, α_1 and α_2, are known. The resulting acceleration vectors at any point make a right angle with their position vector relative to the center of mass. This means that vectors ac_1 and ac_2 make right angles with their position vectors, {Accel_1-G} and {Accel_2-G}, respectively, as G is an instantaneous center of rotation for accelerations. Thus, the angles α_1 and α_2 are obtained through the trigonometric relationship between the components read from the accelerometers.

With these geometric relationships, the problem solution can be set up as the algebraic system of equations in the unknowns dac_{1x} and dac_{2x} (Equation (9)), which correspond to the projected distances from the vehicle's CoG to each accelerometer along the x-axis:

$$\begin{cases} dac_{1x} + dac_{2x} = dac_{12} \\ dac_{1x}cot(\alpha_1) = dac_{2x}cot(\alpha_2) \end{cases} \tag{9}$$

From the previous system of equations, the vertical coordinate of the CoG h_G can be determined in the x-z plane by Equation (10):

$$dac_{1x}/sin(\alpha_1) = dac_{2x}sin(\alpha_2) = h_G \tag{10}$$

2.1.2. CoG Estimation (y-z plane) by Transverse Accelerations

In order to obtain all the CoG coordinates, a complementary method is proposed. The vehicle model is subjected to a cornering maneuver, and the accelerations (due mainly to centrifugal effects and roll motion) are recorded. Also, like in the previous scenario, two sensors are installed at a prescribed distance, but now along the (Y_0) axis, as illustrated below (Figure 5).

The analytical expressions used to estimate the CoG for this method (cornering maneuver, y-z plane) are similar to the ones described above for the straight line trajectory (Equation (11)). The solution is achieved using a similar system of equations, but now adapted to the y-z plane:

$$\begin{cases} dac_{1y} + dac_{2y} = dac_{12} \\ dac_{1y}cot(\alpha_1) = dac_{2y}cot(\alpha_2) \end{cases} \tag{11}$$

From the previous system of equations, the vertical coordinate of the CoG h_G can be determined in the y-z plane by Equation (12):

$$dac_{1y}/sin(\alpha_1) = dac_{2y}sin(\alpha_2) = h_G \tag{12}$$

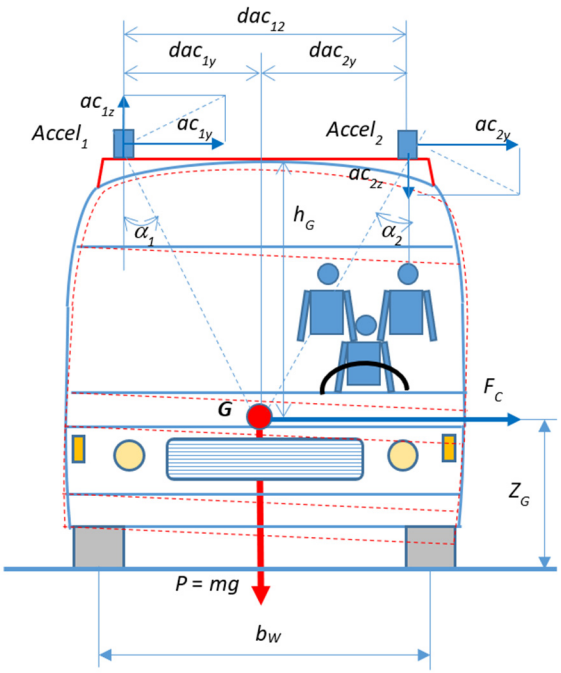


Figure 5. Illustration of the vehicle's geometry in a cornering motion.

It is important to note that the curved trajectory must be known, yet the radius may vary, while the vehicle must run at a constant tangential velocity. Under these conditions, the acceleration components will consist of a set of vertical and radial components, which enable the determination of the center of gravity coordinates on a transverse plane of the vehicle (y-z plane).

2.2. Experimental Method

This study aims to experimentally assess the vehicle's CoG position, with the objective of validating the accuracy of the proposed in-motion methodology. The results obtained from the in-motion road tests will be compared with the results from the static tests, which represent the real values for the CoG position.

2.2.1. Vehicle

A prototype RC-vehicle (characteristics summarized in Table 1) was used for the road tests (Figure 6). The vehicle was suitably adapted to evaluate different driving scenarios and load conditions. It is not equipped with integrated sensors and uses conventional steel coil springs.

Table 1. Vehicle characteristics (RC-vehicle).

Characteristics	Value
Length	0.445 m
Wheelbase	0.325 m
Width	0.269 m
Track	0.228 m
Height	0.141 m
Wheel radius	0.05 m
Mass (empty)	4.43 kg

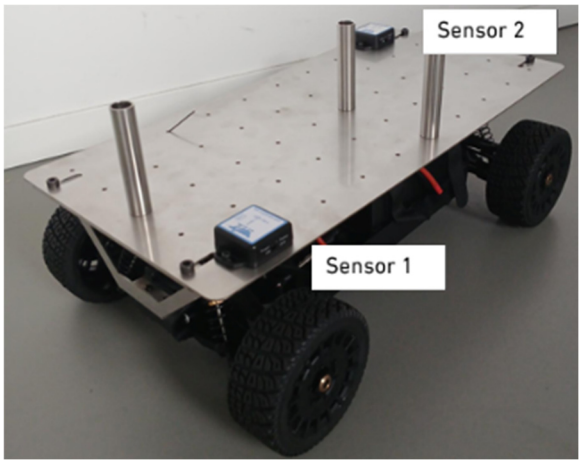


Figure 6. Prototype RC vehicle with sensors installed.

To achieve stable and reproducible results, five load scenarios were defined by placing a 0.751 kg mass in different positions. These cases are shown in Figure 7.

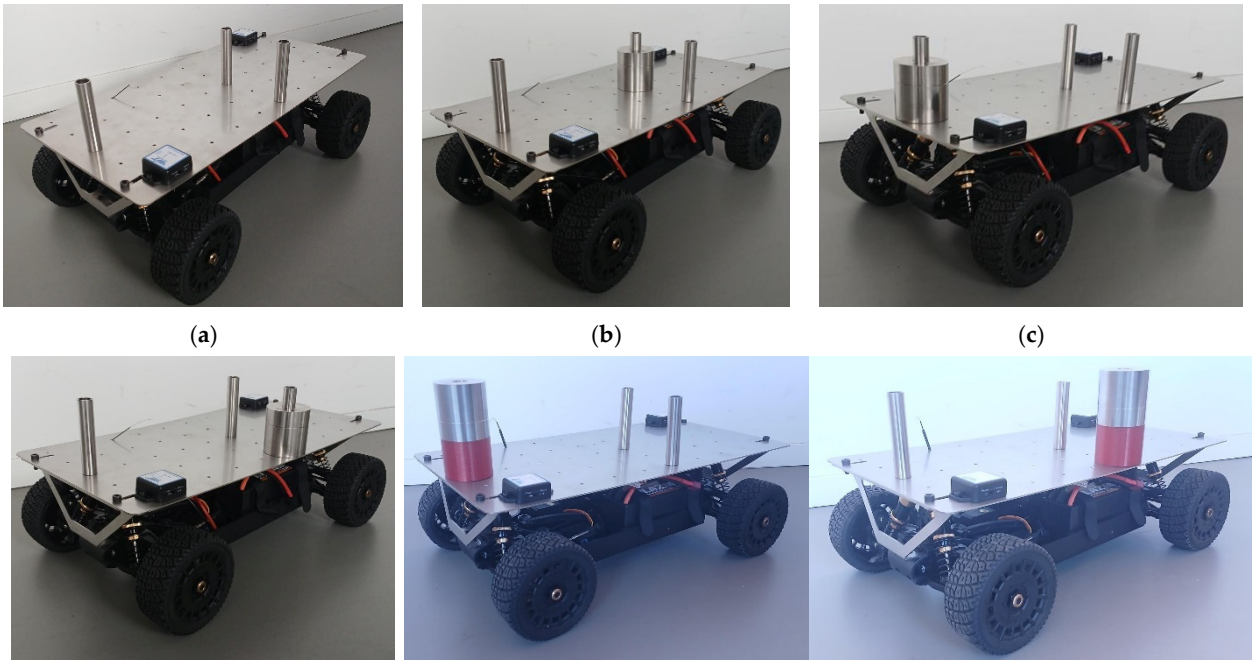


Figure 7. Load case scenarios: (**a**) Load case: empty; (**b**) Load case 1; (**c**) Load case 2; (**d**) Load case 3; (**e**) Load case 4; (**f**) Load case 5.

2.2.2. Static Setup

The purpose of the static measurement method is to determine the actual CoG position of the vehicle, which will be used to validate the results from the dynamic methods.

A laboratory setup was created to measure the weight of the vehicle at each wheel, using the mathematical formulation described earlier. Four load cells (5 kg with amplifier boards: JOY-IT SEN-HX711-05) were used, and the signals were recorded with a National Instruments (NI) DAQ system and associated software.

The vehicle's CoG position in the three directions (x_G, y_G, and z_G) can be determined using basic static equilibrium. The following expressions were applied to obtain the

reference position for each direction. To estimate the CoG height, the lifting method was employed [18].

$$x_G = \frac{R_{Rear} \times w_{Base}}{R_{Front} + R_{Rear}} = \frac{2R_{Rear} \times w_{Base}}{m \times g} \quad (13)$$

$$y_G = \frac{\left(R_{Front_Right} + R_{Rear_Right}\right) \times b_W}{m \times g} \quad (14)$$

$$z_G = \frac{W_{GR} \times \cos\theta + \frac{R_R}{m_{vehicle} \times g} \times W_{base} \times \cos\theta}{\sin\theta} \quad (15)$$

Legend: m—vehicle mass (kg); g—gravitational acceleration $\left(\mathrm{m/s^2}\right)$; b_W—vehicle's track; w_{Base}—vehicle's wheelbase; R_{Front_left}; R_{Front_right}; R_{Rear_left} and R_{Rear_right}—vehicle wheel reactions on ground; W_{GF} and W_{GR}—center of mass position to vehicle axis.

2.2.3. In-Motion Setup

To estimate the vehicle's CoG position in the x-z plane, Equations (9) and (10) are applied, on the other hand, to estimate the vehicle's CoG position in the y-z plane, Equations (11) and (12) are used.

Depending on the equations required to evaluate the CoG position, the accelerations (a_x, a_y, a_z) are the only parameters that need to be measured.

Despite the methodology proposed, it is not necessary to know the vehicle characteristics to evaluate the CoG position, with the sensors' location and their relative position to the vehicle as the only parameters necessary to consider. For the setup used in the prototype vehicle for the data acquisition, sensor 1— the front sensor—was installed:

- In line, approximately 0 mm relative to the left front wheel center in the longitudinal axis;
- It was −0.0175 m relative to the left front wheel (measured to the inside face of the wheel) in the lateral axis.

Sensor 2— the rear sensor—was installed:

- It was 0.0175 m relative to the right front wheel center (outside) in the longitudinal axis;
- It was −0.0250 m relative to the right front wheel track (inside) in the lateral right axis.

The distance between the two sensors is as follows:

- The longitudinal axis (x-axis) is 0.334 m;
- A total of 0.170 m in the lateral axis (y-axis);
- The height relative to the floor (z-axis) is 0.150 m.

In order to obtain those values, the prototype vehicle was equipped with two IMUs (Witmotion WT901BLECL AHRS IMU; WitMotion Shenzhen Co., Ltd., Shenzhen, Guangdong, China), which measure the accelerations, the angular velocity, and the angles in the three axes (see Figure 6). The equipment's x-axis was aligned with the vehicle's movement. Data were sampled at 200 Hz, as it was the maximum acquisition frequency of the selected accelerometers. Using the maximum available sampling rate allowed us to retain as much information as possible in the measured signals for subsequent post-processing. A rate of 200 Hz also provided sufficient resolution to study the phenomena of interest. A smoothing filter—a Butterworth 2nd-order low-pass filter—was applied to improve results visualization.

The algorithm was developed using MATLAB® version R2020a (MathWorks, Natick, MA, USA).

3. Results

This chapter presents all the results for estimating the vehicle's center of gravity (CoG). First, the static results are presented, based on the controlled stationary measurements.

Then, the results from the dynamic methods are shown, using the vehicle's response during braking and cornering tests.

3.1. Static Results

The results from the static measurements, which present the actual CoG position for each load case scenario, are summarized in Table 2. These were the values used as a comparison to those obtained from in-motion tests. All CoG position coordinates were obtained using Equations (13)–(15). Note that x_G was measured from the rear axle, y_G from the left side, and z_G from the ground.

Table 2. Results from static CoG measurements for each load case scenario.

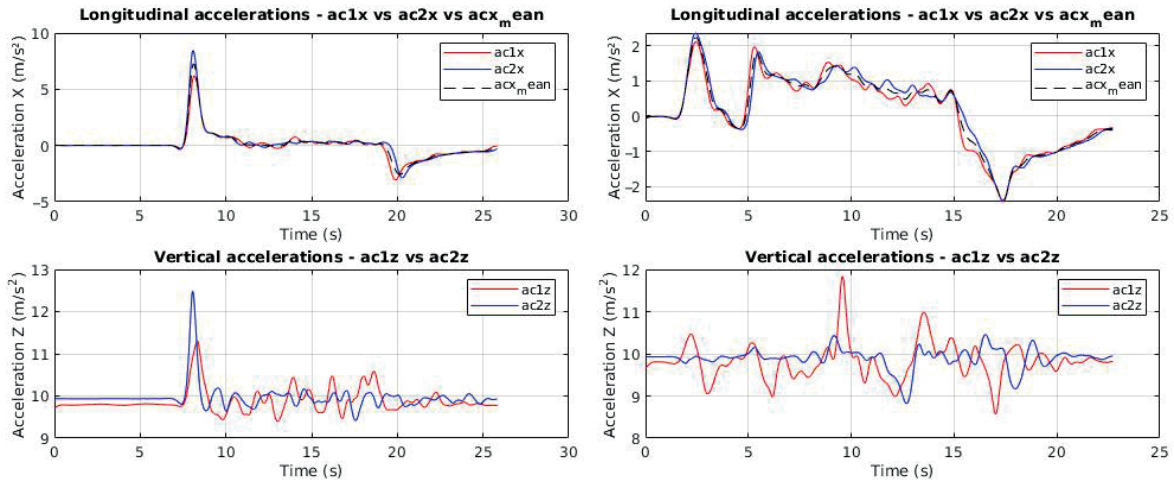
Vehicle Load Variant	x_G [m]	y_G [m]	z_G [m]
Load case: empty	0.1541	0.1175	0.1017
Load case 1	0.1519	0.1150	0.1026
Load case 2	0.1840	0.1181	0.1047
Load case 3	0.1514	0.1068	0.1068
Load case 4	0.1864	0.1180	0.1194
Load case 5	0.1528	0.1076	0.1170

3.2. In-Motion Results

To verify the accuracy of the developed method for estimating the vehicle's CoG position, a series of road tests was conducted with the RC-prototype car. The braking maneuvers were intended to estimate the CoG position in the x-z plane. On the other hand, the cornering maneuvers were intended to estimate the CoG position in the y-z plane. During the road tests, it was important to create significant pitch/roll movements, as well as significant longitudinal, vertical, and lateral accelerations, in order to apply the developed method.

3.2.1. Braking Motion Results

The data obtained from the braking road tests, for all load case scenarios previously defined, are presented in Figure 8. The results for all the load case scenarios are presented in Tables 3 and 4, for the xG and zG positions, respectively.



(**a**) (**b**)

Figure 8. *Cont.*

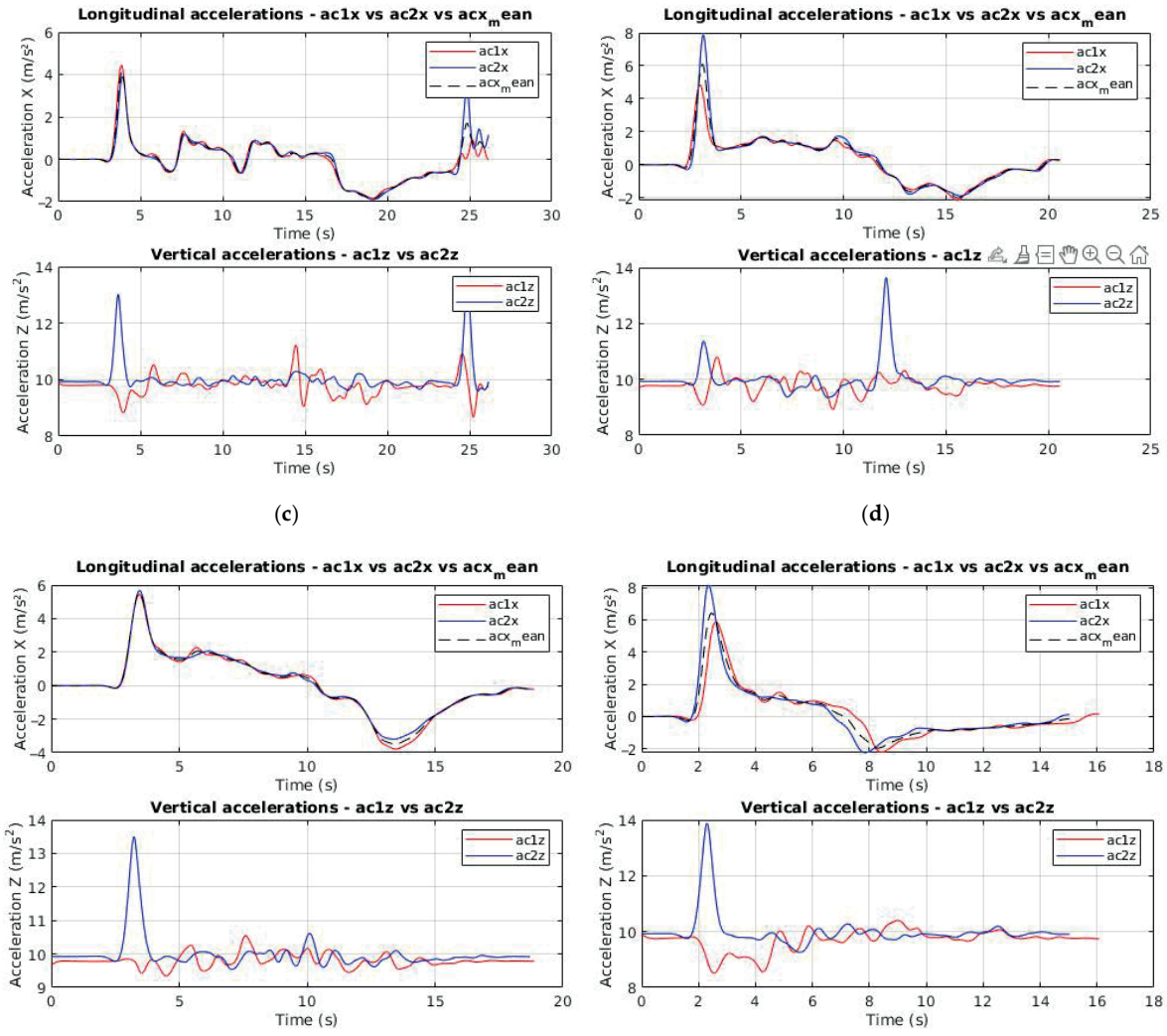


Figure 8. Longitudinal and vertical acceleration data during the in-motion tests: (**a**) empty; (**b**) load case 1; (**c**) load case 2; (**d**) load case 3; (**e**) load case 4; and (**f**) load case 5. (**a**) Maximum braking (~20 s). The average value for the longitudinal acceleration was 2.93 $\frac{\mathrm{m}}{\mathrm{s}^2}$. The vertical acceleration measured in accelerometer 1 was 9.67 $\mathrm{m/s^2}$, while in accelerometer 2 was 9.99 $\mathrm{m/s^2}$. The CoG longitudinal position x_G obtained was 0.152 m (0.0% error), and the CoG vertical position z_G obtained was 0.100 m (0.59% error). (**b**) Maximum braking (~17 s). The average value for the longitudinal acceleration was 2.39 $\frac{\mathrm{m}}{\mathrm{s}^2}$. The vertical acceleration measured in accelerometer 1 was 8.57 $\mathrm{m/s^2}$, while in accelerometer 2 was 10.45 $\mathrm{m/s^2}$. The CoG longitudinal position x_G obtained was 0.166 m (9.71% error), and the CoG vertical position z_G obtained was 0.108 m (4.63% error). (**c**) Maximum braking (~18 s). The average value for the longitudinal acceleration was 1.87 $\frac{\mathrm{m}}{\mathrm{s}^2}$. The vertical acceleration measured in accelerometer 1 was 9.13 $\mathrm{m/s^2}$, while in accelerometer 2 was 10.20 $\mathrm{m/s^2}$. The CoG longitudinal position x_G obtained was 0.159 m (13.38% error), and the CoG vertical position z_G obtained was 0.118 m (3.47% error). Acceleration phase (~4 s). The average value for the longitudinal acceleration was 4.01 $\frac{\mathrm{m}}{\mathrm{s}^2}$. The vertical acceleration measured in accelerometer 1 was 8.82 $\mathrm{m/s^2}$, while in accelerometer 2 was 12.95 $\mathrm{m/s^2}$. The CoG longitudinal position x_G obtained was 0.181 m (1.17% error), and the CoG vertical position z_G obtained was 0.087 m (24.24% error). (**d**) Maximum braking (~16 s). The average value for the longitudinal acceleration was 2.00 $\frac{\mathrm{m}}{\mathrm{s}^2}$. The vertical acceleration measured in accelerometer 1 was 9.41 $\mathrm{m/s^2}$, while in accelerometer 2 was 10.11 $\mathrm{m/s^2}$. The CoG longitudinal position x_G obtained was 0.156 m (2.78% error), and the CoG vertical position z_G obtained was 0.116 m (5.71% error). (**e**) Maximum braking (~10.5 s). The average value for the longitudinal acceleration was 3.49 $\frac{\mathrm{m}}{\mathrm{s}^2}$. The vertical acceleration measured in accelerometer 1 was 9.55 $\mathrm{m/s^2}$, while in accelerometer 2 was 10.10 $\mathrm{m/s^2}$. The CoG longitudinal position x_G obtained was 0.154 m (16.08% error), and the CoG

vertical position z_G obtained was 0.091 m (24.42% error). Acceleration phase (~3 s). The average value for the longitudinal acceleration was 5.51 $\frac{m}{s^2}$. The vertical acceleration measured in accelerometer 1 was 9.42 m/s^2, while in accelerometer 2 was 13.49 m/s^2. The CoG longitudinal position x_G obtained was 0.179 m (2.47% error), and the CoG vertical position z_G obtained was 0.07 m (41.94% error). (**f**) Maximum braking (~8 s). The average value for the longitudinal acceleration was 2.33 $\frac{m}{s^2}$. The vertical acceleration measured in accelerometer 1 was 9.66 m/s^2, while in accelerometer 2 was 10.08 m/s^2. The CoG longitudinal position x_G obtained was 0.153 m (0.52% error), and the CoG vertical position z_G obtained was 0.112 m (2.91% error).

Table 3. CoG longitudinal x_G estimation position for the braking maneuver.

Vehicle Load Variant	x_G Real [m]	x_G Estimation [m]	Absolute Error [m]	Percentage Error [%]
Load case: empty	0.152	0.152	0.000	0.0
Load case 1	0.151	0.166	0.015	9.71
Load case 2	0.183	0.159	0.024	13.38
Load case 2 (Acc)	0.183	0.181	0.002	1.17
Load case 3	0.151	0.156	0.005	2.78
Load case 4	0.184	0.154	0.030	16.08
Load case 4 (Acc)	0.184	0.179	0.005	2.47
Load case 5	0.152	0.153	0.001	0.52

Table 4. CoG height z_G estimation position for the braking maneuver.

Vehicle Load Variant	z_G Real [m]	z_G Estimation [m]	Absolute Error [m]	Percentage Error [%]
Load case: empty	0.100	0.100	0.000	0.59
Load case 1	0.113	0.108	0.005	4.63
Load case 2	0.114	0.118	0.004	3.47
Load case 2 (Acc)	0.114	0.087	0.027	24.24
Load case 3	0.110	0.116	0.006	5.71
Load case 4	0.120	0.091	0.029	24.42
Load case 4 (Acc)	0.120	0.070	0.050	41.94
Load case 5	0.116	0.112	0.004	2.91

3.2.2. Cornering Motion Results

The data obtained from the braking road tests, for all load case scenarios previously defined, are presented in Figure 9. The results obtained for all the load case scenarios are presented in Tables 5 and 6, for the yG and zG position, respectively.

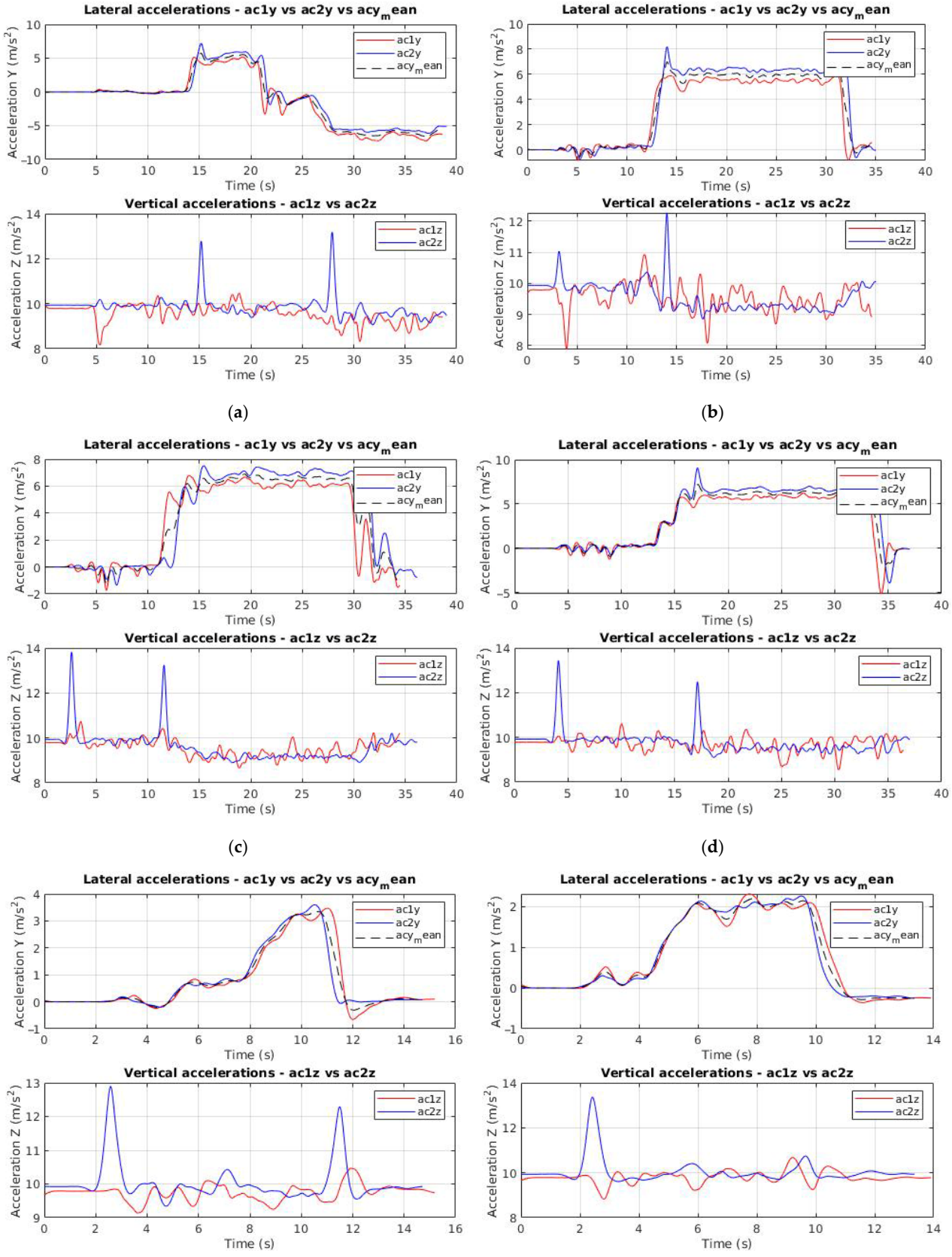


Figure 9. Lateral and vertical accelerations data during in-motion tests: (**a**) empty; (**b**) load case 1; (**c**) load case 2; (**d**) load case 3; (**e**) load case 4; and (**f**) load case 5. (**a**) Maximum lateral acceleration (~15 s). The average value for the lateral acceleration was 6.12 $\frac{m}{s^2}$. The vertical acceleration measured in accelerometer 1 was 9.47 m/s^2, while in accelerometer 2 was 12.60 m/s^2. The CoG lateral position

y_G obtained was 0.113 m (3.46% error), and the CoG vertical position z_G obtained was 0.103 m (3.24% error). (**b**) Maximum lateral acceleration (~14 s). The average value for the lateral acceleration was 6.13 $\frac{m}{s^2}$. The vertical acceleration measured in accelerometer 1 was 9.13 m/s^2, while in accelerometer 2 was 12.22 m/s^2. The CoG lateral position y_G obtained was 0.113 m (3.18% error), and the CoG vertical position z_G obtained was 0.101 m (10.58% error). (**c**) Maximum lateral acceleration (~12 s). The average value for the lateral acceleration was 5.71 $\frac{m}{s^2}$. The vertical acceleration measured in accelerometer 1 was 9.44 m/s^2, while in accelerometer 2 was 12.41 m/s^2. The CoG lateral position y_G obtained was 0.113 m (4.91% error), and the CoG vertical position z_G obtained was 0.106 m (7.20% error). (**d**) Maximum lateral acceleration (~17 s). The average value for the lateral acceleration was 6.20 $\frac{m}{s^2}$. The vertical acceleration measured in accelerometer 1 was 9.38 m/s^2, while in accelerometer 2 was 12.13 m/s^2. The CoG lateral position y_G obtained was 0.114 m (6.55% error), and the CoG vertical position z_G obtained was 0.101 m (7.76% error). (**e**) Maximum lateral acceleration (~11 s). The average value for the lateral acceleration was 3.41 $\frac{m}{s^2}$. The vertical acceleration measured in accelerometer 1 was 9.47 m/s^2, while in accelerometer 2 was 12.26 m/s^2. The CoG lateral position y_G obtained was 0.114 m (3.40% error), and the CoG vertical position z_G obtained was 0.123 m (2.65% error). (**f**) Maximum lateral acceleration (~10 s). The average value for the lateral acceleration was 2.10 $\frac{m}{s^2}$. The vertical acceleration measured in accelerometer 1 was 9.28 m/s^2, while in accelerometer 2 was 10.37 m/s^2. The CoG lateral position y_G obtained was 0.120 m (11.76% error), and the CoG vertical position z_G obtained was 0.132 m (13.91% error).

Table 5. CoG lateral y_G estimation position for the cornering maneuver.

Vehicle Load Variant	y_G Real [m]	y_G Estimation [m]	Absolute Error [m]	Percentage Error [%]
Load case: empty	0.117	0.113	0.004	3.46
Load case 1	0.116	0.113	0.003	3.18
Load case 2	0.119	0.113	0.006	4.91
Load case 3	0.107	0.114	0.007	6.55
Load case 4	0.118	0.114	0.004	3.40
Load case 5	0.108	0.120	0.012	11.76

Table 6. CoG height z_G estimation position for the cornering maneuver.

Vehicle Load Variant	z_G Real [m]	z_G Estimation [m]	Absolute Error [m]	Percentage Error [%]
Load case: empty	0.100	0.103	0.003	3.24
Load case 1	0.113	0.101	0.012	10.58
Load case 2	0.114	0.106	0.008	7.20
Load case 3	0.110	0.101	0.009	7.76
Load case 4	0.120	0.123	0.003	2.65
Load case 5	0.116	0.132	0.016	13.91

3.2.3. Discussion

Regarding the braking maneuver for estimating the CoG position in the x-z plane, the results for the longitudinal coordinate x_G showed good accuracy. Errors were below 10% for the empty load case, load case 1, load case 3, and load case 5. For the load cases where the mass was placed at the front of the vehicle (load case 2 and load case 4), the braking-based estimation presented larger errors of around 15%. However, when the estimation was performed considering the acceleration phase instead of braking, the accuracy of x_G

improved significantly. This can be explained by the effect of torque around the front axle: when the CoG shifts forward due to the additional masses (load case 2 and 4), braking induces a pitch that reduces the influence of the rear axle on the overall load distribution, accentuated by the regular vehicular behavior during braking where the load of the mass of the vehicle is shifted forwards towards the front axle. However, under forward acceleration from a stationary point, the vehicle tilts backward, inducing a load transfer towards the rear axle.

For the vertical position z_G estimated under braking, the method yielded errors below 5% in most cases, except for load case 4, where the error was about 25%. This suggests that elevated front loading introduces dynamics (e.g., suspension deflection and pitch effects) that are not fully captured by the simplified model.

Concerning the cornering maneuver, which aims to estimate the CoG position in the y-z plane, the results for the y_G position were consistent for load cases without vehicle asymmetry. In the asymmetric cases (load cases 3 and 5), the method correctly indicated that a lateral displacement of the CoG occurred, although the precision was limited and the direction of the shift was estimated incorrectly. On the other hand, for the vertical coordinate z_G under cornering, the method successfully detected increases in CoG height when elevated loads were added (cases 4 and 5), even though the error reached 14% in load case 5. For the remaining cases, the estimated z_G values remained in a narrow range, and the method could not clearly distinguish the variations between the empty vehicle and load cases 1, 2, and 3.

An interesting feature would be to combine the braking and cornering approaches. For example, in load case 4, combining both methods could potentially provide precise CoG estimates in all three directions.

The weakest performance of the proposed method was observed in the load cases where the additional loads were placed laterally, which may be explained by the small vehicle dimensions, being unable to detect sufficient acceleration variation, especially on the shortest side of the vehicle.

4. Conclusions

Considering the importance of accurately estimating the center of gravity (CoG) position in both real-time vehicle dynamics control and post-accident vehicular reconstruction analysis, this study presented a practical methodology to estimate a vehicle's CoG using two low-cost inertial measurement units (IMUs) based on the relationship between accelerations measured during motion.

Two different estimation models were developed from vehicle dynamics principles: a longitudinal model to determine the CoG position in the x-z plane during braking, and a roll model to estimate the CoG position in the y-z plane during cornering. To validate these models, experimental tests were conducted using a prototype vehicle equipped with the IMUs under different load conditions. The in-motion results were compared against static measurements, taken as the reference CoG values.

The results showed good accuracy for estimating the longitudinal CoG position x_G, with errors below 10% except for front-loaded cases, where acceleration-phase data should be used instead of the braking-phase data. For the estimation of the vertical position z_G, errors were generally within 5%, with the exception of the front-loaded elevated case during cornering. On the other hand, the estimation of the lateral CoG position y_G presented limited accuracy regarding the load cases with asymmetric loads.

Despite the limitations mentioned for the y_G estimation position, the results obtained validated the applicability of the proposed method for real-world scenarios, offering a practical and scalable approach for onboard CoG estimation under diverse operational contexts.

Future work should focus on integrating the two approaches into a single continuous approach, where lateral acceleration monitoring activates the most suitable estimation strategy, which may improve robustness and accuracy of the results. Moreover, it would be interesting to expand the complexity of the method by including in the analysis the neglected term of the centripetal acceleration. Additionally, the method's validation on full-scale vehicles is recommended to produce larger CoG shifts, enable more repeatable maneuvers, yield stronger acceleration signatures, and better capture real suspension/compliance effects, thereby addressing the discrimination limits observed on the small-scale model.

Author Contributions: Conceptualization, F.C.; methodology, F.C. and F.Q.d.M.; software, F.C., J.S., J.N., and P.J.S.; validation, F.C. and D.F.; formal analysis, F.C.; investigation, F.C. and D.F.; resources, P.M.G.P.M.; writing—original draft preparation, F.C.; writing—review and editing, F.Q.d.M. and D.F.; visualization, F.C.; supervision, P.J.S., M.A.P.V., and P.M.G.P.M.; project administration, F.C. All authors have read and agreed to the published version of the manuscript.

Funding: This research received no external funding.

Institutional Review Board Statement: Not applicable.

Informed Consent Statement: Not applicable.

Data Availability Statement: The data presented in this study are available on request from the corresponding author.

Conflicts of Interest: The authors declare no conflicts of interest.

References

1. Echaveguren, T.; Cruz, P.; Echaveguren, T.; González, P. Estimation of Heavy Vehicle Rollover Potential Using Reliability Principles. *Rev. Ing. Construcción* **2017**, *32*, 5–14.
2. Trigell, A.S.; Rothhämel, M.; Pauwelussen, J.; Kural, K. Advanced vehicle dynamics of heavy trucks with the perspective of road safety. *Veh. Syst. Dyn.* **2017**, *55*, 1572–1617. [CrossRef]
3. Sokolovskij, E.; Žuraulis, V. Advances in Vehicle Dynamics and Road Safety: Technologies, Simulations, and Applications. *Appl. Sci.* **2024**, *14*, 3735. [CrossRef]
4. Rievaj, V.; Vrábel, J.; Synák, F.; Bartuška, L. The Effects of Vehicle Load on Driving Characteristics. *Adv. Sci. Technol. Res. J.* **2018**, *12*, 142–149. [CrossRef] [PubMed]
5. Gupta, A.; Rastogi, V. Effects of Various Road Conditions on Dynamic Behaviour of Heavy Road Vehicle. In *Procedia Engineering*; Elsevier Ltd.: Amsterdam, The Netherlands, 2016; pp. 1129–1137. [CrossRef]
6. Tian, J.; Whitfield, C. Effect of mass and center of gravity on vehicle speed and braking performance. *J. Emerg. Investig.* **2021**, *4*, 1–7. [CrossRef] [PubMed]
7. Castro, F.; de Melo, F.Q.; Faria, D.; Ramos, N.V.; Moreira, P.M.G.P.; Vaz, M.A.P. The Dynamic Behavior of Heavy Vehicles in Cornering Actions: An Assessment of the Problem. *Appl. Sci.* **2025**, *15*, 11959. [CrossRef]
8. Wittmer, K.; Sawodny, O.; Henning, K.U. Model-Based Estimation of Vehicle Center of Gravity Height and Load. *J. Dyn. Syst. Meas. Control Trans. ASME* **2023**, *145*, 051001. [CrossRef]
9. Yang, X.; Wu, C.; He, Y.; Lu, X.Y.; Chen, T. A Dynamic Rollover Prediction Index of Heavy-Duty Vehicles with a Real-Time Parameter Estimation Algorithm Using NLMS Method. *IEEE Trans. Veh. Technol.* **2022**, *71*, 2734–2748. [CrossRef]
10. Cairano, D.; Berntorp, K.; Chakrabarty, A.; Di Cairano, S. Vehicle Center-of-Gravity Height and Dynamics Estimation with Uncertainty Quantification by Marginalized Particle Filter. In Proceedings of the 2021 American Control Conference (ACC), Online, 25–28 May 2021; IEEE: New York, NY, USA, 2021; pp. 160–165. [CrossRef]
11. Park, G.; Choi, S.B. An Integrated Observer for Real-Time Estimation of Vehicle Center of Gravity Height. *IEEE Trans. Intell. Transp. Syst.* **2021**, *22*, 5660–5671. [CrossRef]
12. Wang, C.; Wang, Z.; Zhang, L.; Cao, D.; Dorrell, D.G. A Vehicle Rollover Evaluation System Based on Enabling State and Parameter Estimation. *IEEE Trans Ind. Inf.* **2021**, *17*, 4003–4013. [CrossRef]
13. Boada, B.L.; Garcia-Pozuelo, D.; Boada, M.J.L.; Diaz, V. A Constrained Dual Kalman Filter Based on pdf Truncation for Estimation of Vehicle Parameters and Road Bank Angle: Analysis and Experimental Validation. *IEEE Trans. Intell. Transp. Syst.* **2016**, *18*, 1006–1016. [CrossRef]

14. Rajamani, R.; Piyabongkarn, D.; Tsourapas, V.; Lew, J.Y. Parameter and state estimation in vehicle roll dynamics. *IEEE Trans. Intell. Transp. Syst.* **2011**, *12*, 1558–1567. [CrossRef]
15. Huang, X.; Wang, J. Center of gravity height real-time estimation for lightweight vehicles using tire instant effective radius. *Control Eng. Pract.* **2013**, *21*, 370–380. [CrossRef]
16. Huang, J.; Lin, W.C. EKF-based in-vehicle estimation of relative CG height. In Proceedings of the 2008 ASME Dynamic Systems and Control Conference, DSCC 2008, Ann Arbor, MI, USA, 20–22 October 2008; pp. 295–302. [CrossRef]
17. Solmaz, S.; Akar, M.; Shorten, R.; Kalkkuhl, J. Realtime Multiple-Model Estimation of Center of Gravity Position in Automotive Vehicles. *Veh. Syst. Dyn.* **2008**, *46*, 763–788. [CrossRef]
18. Yue, H.; Zhang, L.; Shan, H.; Liu, H.; Liu, Y. Estimation of the vehicle's centre of gravity based on a braking model. *Veh. Syst. Dyn.* **2015**, *53*, 1520–1533. [CrossRef]
19. Wu, F.; Sun, C.; Li, H.; Zheng, S. Real-Time Center of Gravity Estimation for Intelligent Connected Vehicle Based on HEKF-EKF. *Electronics* **2023**, *12*, 386. [CrossRef]
20. Huang, X.; Wang, J. Real-time estimation of center of gravity position for lightweight vehicles using combined AKF-EKF method. *IEEE Trans. Veh. Technol.* **2014**, *63*, 4221–4231. [CrossRef]
21. Chhoeung, S.; Hahn, A. Approach to estimate the ship center of gravity based on accelerations and angular velocities without ship parameters. In *Journal of Physics: Conference Series*; Institute of Physics Publishing: Bristol, UK, 2019. [CrossRef]
22. Al-Rawashdeh, Y.M.; Elshafei, M.; Al-Malki, M.F. In-Flight Estimation of Center of Gravity Position Using All-Accelerometers. *Sensors* **2014**, *14*, 17567–17585. [CrossRef] [PubMed]
23. Angel, K. *Calculating the Location of the Center-of-Gravity Using an Calculating the Location of the Center-of-Gravity Using an Accelerometer Array Accelerometer Array*; Rochester Institute of Technology: Rochester, NY, USA, 2019; Available online: https://repository.rit.edu/theses (accessed on 17 July 2025).
24. Zhou, J.; Huang, H.; Liu, Y. Spacecraft Center of Mass Online Estimation based on Multi-Accelerometers. In Proceedings of the 2010 2nd IEEE International Conference on Information Management and Engineering, Chengdu, China, 16–18 April 2010; IEEE: New York, NY, USA, 2010. [CrossRef]

Disclaimer/Publisher's Note: The statements, opinions and data contained in all publications are solely those of the individual author(s) and contributor(s) and not of MDPI and/or the editor(s). MDPI and/or the editor(s) disclaim responsibility for any injury to people or property resulting from any ideas, methods, instructions or products referred to in the content.